PAPER

A reduced NiGraf metal organic alloy in the hydrogenation of nitrobenzene to aniline: a computational analysis

Valeria Butera, [ID] *[a] Matteo Formenti, [ID] [b] Giampaolo Barone, [ID] [a] Rosaria Ciriminna,[c] Mario Pagliaro [ID] *[c] and Cristina Della Pina*[b]

Consisting of graphene oxide molecularly entrapped within jamborite nanoparticles, NiGraf (GO@Ni) is a versatile electrocatalyst for both hydrogen and oxygen evolution reactions involved in water electrolysis. Its reduced form obtained *via* reduction of jamborite-entrapped GO with thiophene (RGO@Ni) is a highly active and stable hydrogenation catalyst enabling the reduction of nitrobenzene to aniline at 35 °C in the liquid phase using water as an "on-solvent" reaction medium under biphasic conditions. Besides eliminating the need for an organic solvent, the process has significant practical application potential for the synthesis of a compound produced worldwide at a rate of 7 million tonnes per annum. Here we report the outcomes of a DFT computational study aimed at investigating the catalytic activity and stability of the reduced form of NiGraf in mediating the nitrobenzene hydrogenation to aniline. Results based on calculating the adsorption energies of the two reactant substrates and analyzing the corresponding adsorption modes support a reaction mechanism that explains also the catalyst's remarkable stability.

1. Introduction

Consisting of graphene oxide (GO) molecularly entrapped within jamborite nanoparticles, NiGraf is a metal organic alloy (MORAL) that can be readily deposited at the electrodes of a water electrolyzer to effectively mediate both oxygen and hydrogen evolution reactions.[1] The NiGraf reduced form obtained *via* reduction of GO with thiophene is a highly active and stable catalyst (RGO@Ni) enabling the reduction of nitrobenzene to aniline (benzenamine) at 35 °C under N_2 at atmospheric pressure using water as an "on-solvent" reaction medium under biphasic conditions (eliminating the need for an organic solvent) and a 15 mol% catalytic amount with $NaBH_4$ as a reductant.[2] Furthermore, the catalytic material is highly stable and can be reused to catalyze the reaction without any further treatment for several consecutive reaction runs.

The catalyst (and the enabled mild hydrogenation process) has significant practical application potential for the synthesis of a compound produced worldwide at a rate of 7 million tonnes per annum (growing at a 3% annual growth rate).[3] Aniline indeed is widely employed as a precursor for dyes, agrochemicals, acetaminophen (paracetamol), and methylene diphenyl diisocyanate, as well as an intermediate in polyurethane manufacture.

The chemical industry employs the heterogeneously catalyzed nitrobenzene (NB) hydrogenation carried out either in the vapor phase or in the liquid phase. In the former process NB is fed with hydrogen into a tubular reactor containing a supported Cu catalyst at 270–290 °C and 1–5 bar in the presence of a 9 : 1 (H_2 : NB) excess of hydrogen.[4] The liquid phase process, however, employs supported noble metals (palladium and platinum).[5] Although preferable from a technical viewpoint due to the prevention of harmful hot-spot formation as a consequence of the large reaction exothermicity of >500 kJ mol^{-1}, the latter catalysts are significantly more expensive than the supported Cu catalyst used in the vapor phase reaction.

Ideally, hydrogenation of NB to aniline at completion would be carried out in the liquid phase at low temperature over a solid catalyst employing low-cost supported Ni in place of expensive supported Pt or Pd.

Aiming to test available commercial catalysts suitable for NB hydrogenation in the liquid phase under mild temperature and pressure conditions, in 2016 Madeira and co-workers compared several commercial supported Pd (PdO/Al_2O_3 at three different loadings and different nanoparticle sizes) and Ni (50 wt% NiO/(Al_2O_3 + SiO_2)) catalysts.[6] Results were unequivo-

[a] Dipartimento di Scienze e Tecnologie Biologiche Chimiche e Farmaceutiche, Università di Palermo, viale delle Scienze, Ed.17, 90128 Palermo, Italy. E-mail: valeria.butera@unipa.it

[b] Dipartimento di Chimica, Università di Milano, via Golgi 19, 20133 Milano, Italy. E-mail: cristina.dellapina@unimi.it

[c] Istituto per lo Studio dei Materiali Nanostrutturati, CNR, via U. La Malfa 153, 90146 Palermo, Italy. E-mail: mario.pagliaro@cnr.it

cal: only the Pd-based catalysts gave acceptable selectivity, whereas the Ni-based catalysts promoted substantial formation of secondary products *via* hydrogenolysis and over-hydrogenation of aniline. Furthermore, the reaction conditions were $T = 150$ °C and $P = 14$ bar.

To the best of our knowledge, the most performing Ni-based catalyst reported so far for the liquid phase hydrogenation of NB to aniline is a supported 10 wt% Ni/CB catalyst consisting of 10 nm Ni nanoparticles deposited on mesoporous carbon black (CB) that could achieve nearly 100% conversion of NB to aniline at 120 °C for 60 min under 15 bar H_2. The substantial loss in catalyst already after one reaction run was addressed by heating the used catalyst in a tube furnace at 500 °C for 30 min to reduce the small amount of nickel oxide formed and remove tiny amounts of organic substances deposited on the catalyst.[7] Previously, Hou and co-workers had reported that a Ni/SiO_2 catalyst employed at 15 wt% loading is able to mediate the complete conversion of NB to aniline in EtOH solvent at 90 °C under 10 bar H_2.[8] After six recycles, the Ni nanoparticle size increased from 3.7 to 4.4 nm, indicating that sintering would prevent practical application.

Given the industrial relevance of the NB hydrogenation process, plentiful research has been lately carried out to improve the state-of-the-art methods.[9] In 2005, for example, Jackson in collaboration with catalysis industry researchers demonstrated that the Haber's three-step reaction mechanism (aniline converted to nitrosobenzene, the latter to phenylhydroxylamine, and phenylhydroxylamine to aniline) is wrong.[10] The newly suggested reaction mechanism indicates the formation of Ph–N(OH) as a surface intermediate. Ph–N(OH) would then react either with adsorbed H_2 to form aniline or with itself to eliminate water and produce azoxybenzene.

Concluding the study reporting the discovery of RGO@Ni, we ascribed the remarkable stability of the catalyst to the donation of electrons in the valence band that extends over the whole sheet of graphene to empty d orbitals of Ni.[2] Due to hybridization of the metal d-electrons with the π-orbitals of graphene, graphene and nickel strongly interact with graphene typically lying on the surface of Ni.[11] 3D entrapment of graphene within the Ni metal lattice, however, is completely different from 2D surface adsorption, causing plentiful "side-contacts", namely contacts where Ni atoms interact with graphene edges, leading to the formation of bonds between graphene-edges and nickel.[12]

In this study we conducted a density functional theory (DFT) computational analysis aimed at investigating the catalytic activity and stability of the reduced form of NiGraf in mediating the nitrobenzene hydrogenation to aniline using water as an "on-solvent" reaction medium under biphasic conditions.[2] The presence of the implicit water solvent was mimicked using the conductor-like polarized continuum model (CPCM) method (see below). Results based on calculating the adsorption energies of the two reactant substrates and analyzing the corresponding adsorption modes support a reaction mechanism that explains also the catalyst's remarkable stability.

2. Methods

Reliable prediction of adsorption energies is a key element for the evaluation of the catalytic activity. For example, according to the Brønsted–Evans–Polanyi (BEP) relation for C–C, C–O, C–N, N–O, N–N, and O–O dissociation reactions, the energy barriers of the chemical reactions scale approximately linearly with the adsorption energies of the molecules.[13]

All calculations were performed using the Gaussian 16 (Revision C.01) package.[14] The cluster models were selected based on previous studies on similar systems,[15,16] including Pd-entrapped graphene oxide (GrafeoPlad-Pd) using a similar route to molecularly doped metals.[17] We retained the cluster's overall zero spin and neutral charge by passivating with capping H atoms only the dangling C bonds of reduced GO. We selected the hybrid B3LYP[18,19] functional in conjunction with the fully electron basis set 6-31+G** for all the atoms and the inclusion of Grimme's dispersion with the original D3 damping function.[20] Frequency calculations were conducted to check the nature of the stationary points. We briefly remind that the cluster model approach has been lately shown to be a powerful method to accurately predict adsorption modes and the corresponding adsorption energies in heterogeneous catalysis, and therefore a valid alternative to periodic boundary condition (PBC) calculations.[20,21]

The adsorption energies $E(mol)_{ads}$ are calculated as:

$$E(mol)_{ads} = E_{cluster+mol} - E_{cluster} - E_{mol} \qquad (1)$$

where $E_{cluster}$ is the energy of the optimized cluster, E_{mol} is the energy of the free NB or H_2 molecule, and $E_{cluster+mol}$ is the energy of the cluster when an NB or H_2 molecule is adsorbed on the surface. The presence of the implicit water solvent was mimicked using the CPCM method,[22] by single point calculations on all the optimized structures obtained *in vacuo*.

3. Results and discussion

Ni atomic cluster particles in RGO@Ni were simulated by adding a cluster of 6 Ni atoms below the coronene plane. The outcome of DFT calculations clearly indicates the formation of chemical bonds between Ni and C atoms, whose distances are in the range of 1.97–2.13 Å, and between Ni atoms, with calculated distances within 2.24 and 2.45 Å (Fig. 1).
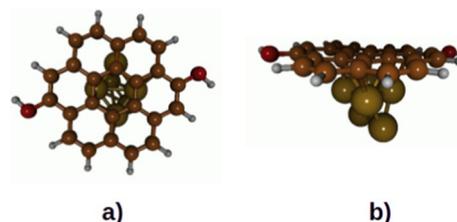

Fig. 1 (a) Top and (b) side view of the optimized structure of RGO@Ni.

However, since experimental findings support that the real system consists of jamborite nanoparticles encapsulating GO platelets,[1] a second model, RGO@Ni(OH)$_2$, whose optimized structure is shown in Fig. 2, was investigated.

In this second model, jamborite cluster particles were simulated by introducing a small cluster of two Ni(OH)$_2$ units, carved out from the Ni(OH)$_2$ crystallographic structure. Interestingly, DFT calculations underline that during the relaxation, the Ni(OH)$_2$ dimer cluster moves closer to the RGO surface and two interactions are established between Ni and C atoms of RGO, whose computed distances are 2.36 and 2.41 Å.

We thus analyzed computationally the catalytic activity of both models in activating nitrobenzene and hydrogen molecule substrates. For both models, we considered the two substrates approaching from the top of the RGO surface or from the bottom side of Ni NPs or the Ni(OH)$_2$ cluster.

Results show that when the H$_2$ molecule approaches the cluster from the top of the RGO plane, it ends up weakly physisorbed on it, as shown by the computed adsorption energy of only −0.07 eV and by the identical calculated H–H bond distance (0.74 Å) with respect to the free molecule. This outcome is the same regardless of whether RGO is entrapped within Ni or Ni(OH)$_2$ clusters (Fig. 3).

NB behaves similarly to H$_2$ when adsorbing on top of RGO in the presence of RGO@Ni and RGO@Ni(OH)$_2$. However, the presence of the benzene ring in NB allows for the establishment of π–π interaction with RGO (Fig. 4), thus leading to a more negative physisorption with respect to the hydrogen molecule.

Moreover, DFT results reveal that NB is more strongly physisorbed on RGO@Ni than on RGO@Ni(OH)$_2$ with an adsorption energy of −0.62 eV in the former case and −0.49 eV in the latter. This is due to the formation of a hydrogen bond between the OH moiety of the RGO and one of the oxygen atoms of the nitro group, and a potential indirect role of Ni atoms in the cluster in enhancing nitrobenzene physisorption.

However, due to the weak activation of the H$_2$ molecule mentioned above, hydrogenation of nitrobenzene cannot take place when both substrates are adsorbed on RGO. On the other hand, when both substrate molecules (H$_2$ and NB) are located in the proximity of Ni atoms in RGO@Ni, strong chemical adsorption takes place in both cases (Fig. 5).

DFT calculations show that during relaxation, NB moves closer to Ni atoms and chemical bonds are established between
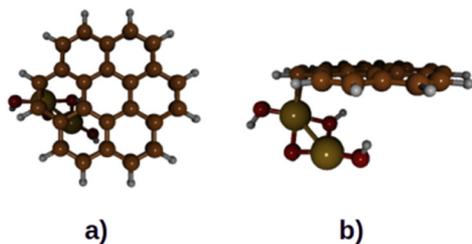

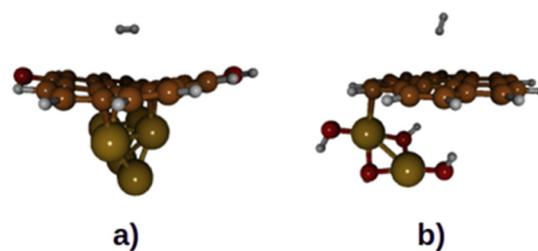Fig. 2   (a) Top and (b) side view of the optimized structure of RGO@Ni(OH)$_2$.

Fig. 3   H$_2$ adsorption on top of RGO in the presence of (a) RGO@Ni (E_{ads} = −0.07 eV) and (b) RGO@Ni(OH)$_2$ (E_{ads} = −0.07 eV).
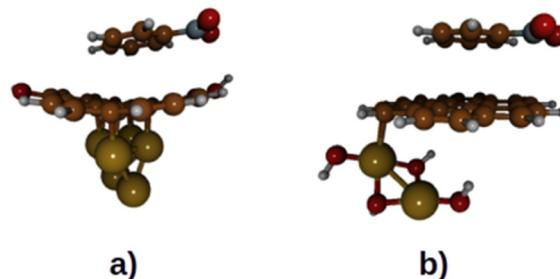

Fig. 4   NB adsorption on top of RGO in the presence of (a) RGO@Ni (E_{ads} = −0.62 eV) and (b) RGO@Ni(OH)$_2$ (E_{ads} = −0.49 eV).
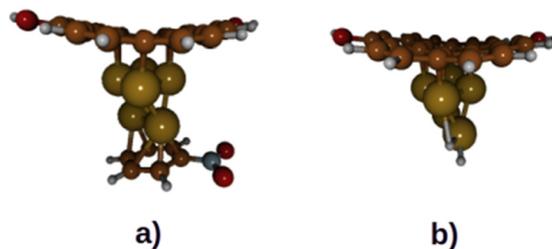

Fig. 5   (a) NB (E_{ads} = −1.53 eV) and (b) H$_2$ (E_{ads} = −0.76 eV) adsorption on Ni atoms in RGO@Ni.

Ni atoms and C atoms of NB. A very negative adsorption energy of −1.53 eV was obtained. Differently from the previous case, the H–H bond in H$_2$ molecule breaks and two Ni–H chemical bonds are formed, with a computed adsorption energy of −0.76 eV. Formation of such strong Ni–H bonds hinders the hydrogen transfer to NB, required in the hydrogenation step, and the subsequent release of the hydrogenated substrate molecule. We briefly remind that the reaction mechanism of NB hydrogenation involves the formation of Ph–N(OH) as a surface intermediate, followed either by a reaction of Ph–N(OH) with adsorbed hydrogen to form aniline or by a dismutation reaction of Ph–N(OH) to eliminate water and produce azoxybenzene that is subsequently, but more slowly, converted to aniline.[10]

Therefore, neither RGO nor Ni NPs in RGO@Ni are potential active sites towards NB hydrogenation.

On the other hand, computational results show that when NB is positioned next to the Ni(OH)$_2$ dimer cluster (Fig. 6a),
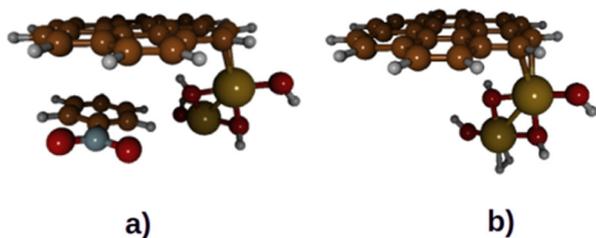
Fig. 6 (a) NB (E_{ads} = −0.60 eV) and (b) H_2 (E_{ads} = −0.33 eV) adsorption on Ni(OH)$_2$ in RGO@Ni(OH)$_2$.

the molecule establishes a π–π interaction with RGO similarly to the cases described earlier. However, thanks to the vicinity of Ni(OH)$_2$ units additional hydrogen bonds between the hydrogen atoms of NB and the OH group of the Ni hydroxide are formed, contributing to further increasing the physisorption and to lowering the adsorption energy, which becomes 0.13 eV more negative with respect to the adsorption on top of RGO in RGO@Ni(OH)$_2$.

When the H_2 molecule approaches the Ni(OH)$_2$ dimer cluster in RGO@Ni(OH)$_2$ it coordinates to the metal center, thereby forming a four-coordinated Ni complex (Fig. 6b). The H–H bond elongates from 0.74 Å in the free molecule to 0.79 Å in the physisorbed molecule, while the calculated Ni–H_2 bond distance is 1.66 Å. Moreover, while in the case of physisorption discussed earlier, the natural bond orbital analysis (NBO) underlines an almost null polarization of the H–H bond (calculated NBO charges of −0.008 and +0.008), and in the latter case, the computed NBO charges of 0.088 and 0.073 highlight enhanced bond polarization. The calculated adsorption energy indeed is −0.33 eV.

Altogether, these findings suggest that Ni(OH)$_2$, and not Ni atomic cluster particles, acts as an optimal catalytically active site for the adsorption and activation of the H_2 molecule in the hydrogenation of NB to aniline mediated by reduced NiGraf molecularly doped metal.

Remarkably, said computational findings are in agreement with the experimental observation of the elemental maps of RGO@Ni following the reduction of NiGraf with thiophene, showing that reduction of GO to graphene using thiophene does not reduce the jamborite nanocrystals to Ni nanoparticles.[2]

In brief, calculations suggest that when employing the RGO@Ni catalyst, there are no Ni nanoparticles but rather the Ni(OH)$_2$ dimer cluster in RGO@Ni(OH)$_2$ whose mechanism of action in mediating the nitrobenzene hydrogenation with H_2 or BH_4^- is analogous to that of nitroarene hydrogenation mediated by Ni(OH)$_2$ nanoparticles deposited on polyaniline nanotubes (transfer to the nitroarene substrate of surface-bound hydrides with rapid desorption of the newly formed aniline).[23]

In the case of the RGO@Ni metal organic alloy (reduced NiGraf), graphene (RGO) binds and keeps close to the RGO surface the Ni(OH)$_2$ dimer clusters thanks to the two interactions between Ni and C atoms of RGO (computed distances are 2.36 and 2.41 Å) whereas the ultramild reaction conditions employed ensure that neither BH_4^- nor H_2 may reduce Ni(OH)$_2$

to metallic Ni nanoparticles. This explains also the exceptional stability of the RGO@Ni catalyst and, indirectly, the poor stability of rapidly agglomerating Ni RANEY® and Ni nanoparticles.

The cluster model approach used in this study is a reliable method to accurately predict adsorption modes and the corresponding adsorption energies to investigate a wide range of catalytic reactions,[15–17] as a valid alternative to PBC calculations. For example, a computational analysis comparing said two complementary computational methods for the investigation of a medium-to-large and complex glucose molecule adsorbed on a specific (100) anatase crystalline plane clearly showed the reliability of smaller cluster models in terms of the geometric parameters, the adsorption energies and the adsorption modes with the more extended TiO$_2$ surfaces obtained by PBC calculations.[24]

4. Conclusions

In conclusion, the findings of the first computational DFT investigation aimed at explaining the exceptional catalytic activity and stability of the reduced form of the NiGraf metal organic alloy in mediating the nitrobenzene hydrogenation to aniline under ambient conditions suggest that:

(i) when H_2 and NB approach the RGO graphene surface in RGO@Ni and RGO@Ni(OH)$_2$, both molecules are only weakly physisorbed and therefore the RGO surface does not act as an active site for the adsorption and activation of both substrates;

(ii) Ni atomic clusters establish overly strong bonds with both NB and H_2, thus preventing the substrates to further react toward the hydrogenation step;

(iii) Ni(OH)$_2$ acts as an active site for the coordination and activation of the H_2 molecule contributing to enhancing the NB adsorption *via* hydrogen bond formation.

Such a reaction mechanism, furthermore, would avoid the common problem observed in Ni nanoparticle catalysis applied to NB hydrogenation, namely, the formation of aniline begins to accelerate when the conversion of NB is greater than 90%, because NB, being strongly adsorbed, inhibits the surface of the Ni cluster or nanoparticles.

Finally, to get a deeper understanding of the catalytic activity of nitrobenzene hydrogenation to aniline mediated by reduced NiGraf, future work will focus on the two competing reaction pathways (direct hydrogenation to aniline and the dismutation to azoxybenzene), with the consequent interception of all the stationary points (intermediates and transition states) involved in each process. When confirmed by further experimental investigations on the reaction mechanism besides the important discovery reported in early 2025,[2] these findings may lead to industrial uptake of reduced NiGraf as the catalyst of choice for the industrial production of aniline *via* nitrobenzene hydrogenation.

Conflicts of interest

There are no conflicts to declare.

Data availability

All data are available upon reasonable request from the corresponding authors.

Acknowledgements

References

1 M. Pagliaro, M. V. Pagliaro, R. Caliandro, C. Giannini, R. Ciriminna and A. Lavacchi, *Mater. Adv.*, 2024, **5**, 2759–2766, DOI: 10.1039/d3ma00700f.

2 M. Formenti, R. Ciriminna, C. Della Pina and M. Pagliaro, *Next Mater.*, 2025, **8**, 100751, DOI: 10.1016/j.nxmate.2025.100751.

3 ChemAnalyst, Aniline Market Analysis: Industry Market Size, Plant Capacity, Production, Operating Efficiency, Demand & Supply, End-User Industries, Sales Channel, Regional Demand, Company Share, Foreign Trade, Manufacturing Process, Policy and Regulatory Landscape, 2015–2032, New York, 2023. https://www.chemanalyst.com/industry-report/aniline-market-282 (accessed 1 December 2025).

4 T. Kahl, K. W. Schröder, F. R. Lawrence, W. J. Marshall, H. Höke and R. Jäckh, *Aniline. Ullmann's Encyclopedia of Industrial Chemistry*, Wiley, New York, 2011. DOI: 10.1002/14356007.a02_303.pub2.

5 M. Turáková, T. Salmi, K. Eränen, J. Wärnå, D. Yu Murzin and M. Králik, *Appl. Catal., A*, 2015, **499**, 66–76, DOI: 10.1016/j.apcata.2015.04.002.

6 C. Sá Couto, L. M. Madeira, C. P. Nunes and P. Araújo, *Appl. Catal., A*, 2016, **522**, 152–164, DOI: 10.1016/j.apcata.2016.04.032.

7 H. Jiang, G. Yuan, Z. Cui, Z. Zhao, Z. Dong, J. Zhang, Y. Cong and X. Li, *Ind. Eng. Chem. Res.*, 2023, **62**, 13355–13367, DOI: 10.1021/acs.iecr.3c01327.

8 J. Wang, Z. Yuan, R. Nie, Z. Hou and X. Zheng, *Ind. Eng. Chem. Res.*, 2010, **49**, 4664–4669, DOI: 10.1021/ie1002069.

9 M. Králik, M. Turáková, I. Mačák and P. Lehocký, Aniline – catalysis and chemical engineering, in *Proceedings of 41st International Conference of Slovak Society of Chemical Engineering*, Tatranské Matliare, Slovakia, 2014, pp. 723–733. https://www.researchgate.net/publication/263010315_Aniline_-_Catalysis_and_Chemical_Engineering.

10 E. A. Gelder, S. D. Jackson and C. Martin Lok, *Chem. Commun.*, 2005, 522–524, DOI: 10.1039/b411603h.

11 A. Dahal and M. Batzill, *Nanoscale*, 2014, **6**, 2548–2562, DOI: 10.1039/c3nr05279f.

12 J. Lahiri and M. Batzill, *Appl. Phys. Lett.*, 2010, **97**, 023102, DOI: 10.1063/1.3464173.

13 S. Wang, B. Temel, J. Shen, G. Jones, L. C. Grabow, F. Studt, T. Bligaard, F. Abild-Pedersen, C. H. Christensen and J. K. Nørskov, *Catal. Lett.*, 2011, **141**, 370–373, DOI: 10.1007/s10562-010-0477-y.

14 M. J. Frisch, G. W. Trucks, H. B. Schlegel, G. E. Scuseria, M. A. Robb, J. R. Cheeseman, G. Scalmani, V. Barone, G. A. Petersson, H. Nakatsuji, X. Li, M. Caricato, A. V. Marenich, J. Bloino, B. G. Janesko, R. Gomperts, B. Mennucci, H. P. Hratchian, J. V. Ortiz, A. F. Izmaylov, J. L. Sonnenberg, D. Williams-Young, F. Ding, F. Lipparini, F. Egidi, J. Goings, B. Peng, A. Petrone, T. Henderson, D. Ranasinghe, V. G. Zakrzewski, J. Gao, N. Rega, G. Zheng, W. Liang, M. Hada, M. Ehara, K. Toyota, R. Fukuda, J. Hasegawa, M. Ishida, T. Nakajima, Y. Honda, O. Kitao, H. Nakai, T. Vreven, K. Throssell, J. A. Montgomery Jr., J. E. Peralta, F. Ogliaro, M. J. Bearpark, J. J. Heyd, E. N. Brothers, K. N. Kudin, V. N. Staroverov, T. A. Keith, R. Kobayashi, J. Normand, K. Raghavachari, A. P. Rendell, J. C. Burant, S. S. Iyengar, J. Tomasi, M. Cossi, J. M. Millam, M. Klene, C. Adamo, R. Cammi, J. W. Ochterski, R. L. Martin, K. Morokuma, O. Farkas, J. B. Foresman and D. J. Fox, *Gaussian 16, Revision C.01*, Gaussian, Inc., Wallingford CT, 2016.

15 V. Butera and H. Detz, *Mater. Chem. Front.*, 2021, **5**, 8206–8217, DOI: 10.1039/d1qm01118a.

16 V. Butera and H. Detz, *ACS Appl. Energy Mater.*, 2022, **5**, 4684–4690, DOI: 10.1021/acsaem.2c00110.

17 M. Formenti, M. P. Casaletto, G. Barone, M. Pagliaro, C. Della Pina, V. Butera and R. Ciriminna, *Adv. Sustainable Syst.*, 2024, **8**, 2300643, DOI: 10.1002/adsu.202300643.

18 A. D. Becke, *J. Chem. Phys.*, 1997, **107**, 8554–8560, DOI: 10.1063/1.475007.

19 A. D. Becke, *J. Chem. Phys.*, 1993, **98**, 5648–5652, DOI: 10.1063/1.464913.

20 S. Grimme, J. Antony, S. Ehrlich and H. Krieg, *J. Chem. Phys.*, 2010, **132**, 154104, DOI: 10.1063/1.3382344.

21 H. Burge, D. Collins and B. Davis, *Ind. Eng. Chem. Prod. Res. Dev.*, 1980, **19**, 3899–3891, DOI: 10.1021/i360075a019.

22 V. Barone and M. Cossi, *J. Phys. Chem. A*, 1998, **102**, 1995–2001, DOI: 10.1021/jp9716997.

23 V. S. Sypu, M. Bhaumik, K. Raju and A. Maity, *J. Colloid Interface Sci.*, 2021, **581**, 979–989, DOI: 10.1016/j.jcis.2020.08.111.

24 V. Butera, A. Massaro, A. B. Muñoz-García, M. Pavone and H. Detz, *Front. Chem.*, 2021, **9**, 716329, DOI: 10.3389/fchem.2021.716329.